Characterization of a Thermostable NADPH:FMN Oxidoreductase from the Mesophilic Bacterium *Bacillus subtilis*†

Sigrid Deller,‡ Sonja Sollner,‡ Rosemarie Trenker-El-Toukhy,‡ Ilian Jelesarov,§ Georg M. Gübitz,|| and Peter Macheroux*,‡

Institute of Biochemistry, Graz University of Technology, Petersgasse 12/II, A-8010 Graz, Austria, Institute of Biochemistry, University of Zürich, CH-8057 Zürich, Switzerland, and Institute of Environmental Biotechnology, A-8010 Graz University of Technology, Graz, Austria

Received December 5, 2005; Revised Manuscript Received April 6, 2006

ABSTRACT: The gene *yhd*A from *Bacillus subtilis* encoding a putative flavin mononucleotide (FMN)-dependent oxidoreductase was cloned and heterologously expressed in *Escherichia coli*. The purified enzyme has a noncovalently bound FMN cofactor, which is preferentially reduced by NADPH, indicating that YhdA is a NADPH:FMN oxidoreductase. The rate of NADPH oxidation is enhanced by the addition of external FMN, and analysis of initial rate measurements reveals the occurrence of a ternary complex in a bi-bi reaction mechanism. YhdA has also been shown to reductively cleave the −N═N− bond in azo dyes at the expense of NADPH, and hence, it possesses azoreductase activity, however, at a rate 100 times slower than that found for FMN. Using Cibacron Marine as a model compound, we could demonstrate that the dye is a competitive inhibitor of NADPH and FMN. The utilization of NADPH and the absence of a flavin semiquinone radical distinguish YhdA from flavodoxins, which adopt the same structural fold, i.e., a five-stranded β sheet sandwiched by five α helices. The native molecular-mass of YhdA was determined to be 76 kDa, suggesting that the protein occurs as a tetramer, whereas the YhdA homologue in *Saccharomyces cerevisiae* (YLR011wp) forms a dimer in solution. Interestingly, the different oligomerization of these homologous proteins correlates to their thermostability, with YhdA exhibiting a melting point of 86.5 °C, which is 26.3 °C higher than that for the yeast protein. This unusually high melting point is proposed to be the result of increased hydrophobic packing between dimers and the additional presence of four salt bridges stabilizing the dimer−dimer interface.

Several bacterial species contain enzymes that utilize either NADH or NADPH to reduce a tightly but noncovalently bound flavin mononucleotide (FMN) or flavin adenine dinucleotide (FAD) cofactor in their active sites. A number of substrates were reported for these enzymes such as FMN, quinones, nitro-organic compounds, and azo dyes (*1*, *2*). The ability to reductively cleave the azo bond has led to the designation as azoreductases (AZRs),[1] although it must be emphasized that these synthetic compounds are not cognate substrates in an original physiological context. However, specialized AZRs have apparently evolved in bacterial species exposed to high concentrations of azo dyes, for example, in wastewater discharges of dyestuff manufacturing or handling industries (*3*).

AZR activity was reported for various bacteria living in as diverse of habitats as soil and the human gastrointestinal tract. The genes encoding for bacterial AZRs were cloned from *Bacillus subtilis* sp. OY1-2 (*4*), *Enterococcus faecalis* (*5*), *Escherichia coli* (*6*), *Pigmentiphaga kullae* (*7*), *Rhodobacter sphaeroides* (*8*), *Staphylococcus aureus* (*9*), and *Xenophilus azovorans* (*10*). Most of these AZRs contain between 180 and 210 amino acids and have on average a molecular mass of 19−23 kDa, with the only exception being the AZR from *Xenophilus azovorans*, which contains 281 amino acids and possesses a molecular mass of 30 kDa. The AZR from the latter species does not share sequence similarity with the other AZRs, suggesting that bacteria have evolved more than one enzyme with AZR activity from different ancestral proteins. The recent isolation of an AZR from *Enterobacter agglomerans* with a molecular mass of 28 kDa provides further support for the existence of at least two unrelated AZR families (*11*). Here, we report the cloning of a gene from *B. subtilis* strain 168, designated *yhd*A, encoding a putative short-chain AZR comprising 178 amino acids with an overall identity of 57% to the AZR reported in *B. subtilis* sp. OY1-2 (*4*).

Several important issues remain controversial with regard to the short-chain AZRs: some were reported as monomers, while others appear to exist as di- or tetramers. Even more puzzling is the question of the presence of a redox cofactor

* To whom correspondence should be addressed: Graz University of Technology, Institute of Biochemistry, Petersgasse 12/II, A-8010 Graz, Austria. Telephone: +43-316-873-6450. Fax: +43-316-873-6952. E-mail: peter.macheroux@tugraz.at.

† This work was supported by the Austrian Fonds zur Förderung der wissenschaftlichen Forschung (FWF), providing a fellowship to S.S. through the Doktoratskolleg "Molecular Enzymology".

‡ Institute of Biochemistry, Graz University of Technology.

§ University of Zürich.

|| Institute of Environmental Biotechnology, Graz University of Technology.

[1] Abbreviations: AZR, azoreductase; IPTG, isopropyl-1-thio-D-galactopyranoside; LOT6, low-temperature-responsive gene 6 (YLR011w); Ni−NTA, nickel−nitrilotriacetic acid agarose.

10.1021/bi052478r CCC: $33.50
Published on Web 05/17/2006

in the active site: in the case of the AZRs from *E. faecalis*, *E. coli*, and *S. aureus*, FMN was reported as a cofactor, while in the case of *Bacillus* sp. OY1-2, *P. kullae*, and *R. sphaeroides*, no cofactor was identified (*4*−*9*). Likewise, no protein-bound cofactor was identified for the two "long-chain" AZRs from *E. agglomerans* and *X. azovorans* (*10*, *11*). The apparent absence of a flavin cofactor from the AZR from *Bacillus* sp. OY1-2 is difficult to reconcile with the available X-ray crystal structure of YhdA from *B. subtilis*, which clearly shows the presence of FMN (PDB entry code 1NNI). Similarly, elucidation of the X-ray crystal structure of a homologous enzyme from *Saccaromyces cerevisiae*, termed low-temperature-responsive gene 6 (YLR011w) (LOT6), demonstrated the presence of FMN in the active site (*12*).

Interestingly, both of these proteins display a common structural topology, known as the flavodoxin-like fold. This fold consists of a central five-stranded parallel β sheet flanked by five α helices and is found in pro- and eukaryotic NAD(P)H:quinone oxidoreductases and so-called flavodoxins. This latter family of proteins is predominantly found in bacteria, where they are involved in various electron-transfer reactions. Flavodoxins have been extensively studied because they possess very pronounced biochemical and spectroscopic properties, such as the stabilization of a neutral flavin semiquinone ("blue radical"). Despite having a similar fold, flavodoxins use tightly bound FMN as a cofactor, whereas NAD(P)H:quinone oxidoreductases specifically bind FAD (*2*). Because bacterial and yeast AZRs adopt a flavodoxin-like fold, it would be very interesting to know how they are related to flavodoxins and NAD(P)H:quinone oxidoreductases in terms of their biochemical and spectroscopic properties.

The presence of a cofactor in AZRs has also mechanistic implications because the cleavage of the nitrogen double bond requires the delivery of a total of four electrons, a reaction that a flavin cofactor could carry out in two sequential reduction (by NADH or NADPH) and oxidation (by the azo compound) steps via a hydrazo intermediate.

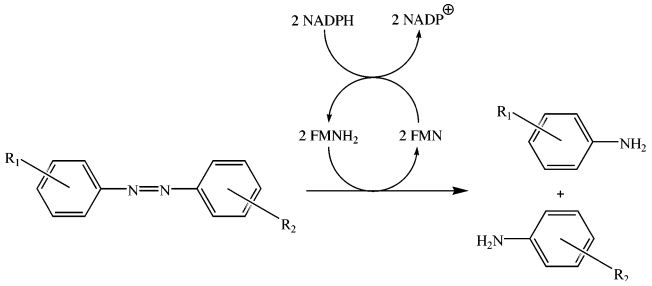

Currently, it is not clear whether AZRs actually possess a substrate-binding pocket that can accommodate azo compounds or the assumed hydrazo intermediate. The propensity of AZRs to bind these compounds would be very intriguing in view of the fact that the cognate substrate of these enzymes is currently unknown and not to mention the functional role of the enzymes.

In light of the biotechnological potential of AZRs and our poor understanding of their biochemical properties as well as physiological function(s), we have initiated the biochemical characterization of the putative AZR from *B. subtilis*, YhdA. Here, we show that YhdA is a NADPH:FMN oxidoreductase, which rapidly reduces FMN in a ternary complex, but a rather poor AZR.

MATERIALS AND METHODS

Reagents. All chemicals were of the highest grade commercially available and purchased from Sigma−Aldrich, Fluka, or Merck. The nickel−nitrilotriacetic acid agarose (Ni−NTA) was from Qiagen, and the HiTrap chelating column was from Pharmacia Biotech AB.

Bacterial Strains and Media. B. subtilis strain 168 was cultivated in Luria−Bertani (LB) medium at 37 °C, and genomic DNA was isolated using the DNA purification kit from Fermentas. For recombinant DNA work, *E. coli* DH5α and *E. coli* BL21 (DE3) were used. For selection of ampicillin-resistant *E. coli* strains, LB medium was supplemented with 100 μg/mL ampicillin. *B. subtilis yhd*A knockout strain (BFS1650) was kindly provided by Dr. Kazuo Kobayashi, Nara Institute of Science and Technology, Japan. A preculture (LB medium, 10 mL) was inoculated from a glycerol stock and incubated at 37 °C overnight. This culture was used to inoculate 500 mL of LB medium. The culture was grown until an $OD_{600} = 0.6$, and cells were harvested by centrifugation. The pellet was washed with 50 mM phosphate buffer at pH 7.0, resuspended, and incubated with 2.5 mg of lysozyme for 1 h at 4 °C under slight stirring. Afterward, the suspension was centrifuged again and washed with phosphate buffer.

Cloning of yhdA from B. subtilis and Expression in E. coli. The *yhd*A gene was amplified by the polymerase chain reaction (PCR) using genomic DNA isolated from *B. subtilis* strain 168 as a template. The forward primer contained a *Nde*I (5′-GGAATTCCATATGGAATTCCATGAACATG-TTAGTCATAAATGGC-3′), and the reverse primer contained a *Xho*I restriction site (5′-CCGCTCGAGCGGGACGC-CGGGATTTCCTG-3′), respectively. The reverse primer was designed without a stop codon, which allows for the expression of the protein with a C-terminal hexahistidine-affinity tag. The PCR product was directly cloned into the *Nde*I/*Xho*I restriction sites of the pET21a vector (Novagen) generating the expression plasmid pETyhdA. Chemically competent *E. coli* DH5α cells were transformed with the pETyhdA. After transformation, the sequence of the transformation construct was verified by sequencing analysis. For expression of YhdA, the host expression strain *E. coli* BL21 was subsequently transformed with the purified plasmid.

Expression of YhdA was achieved by growing a 10 mL preculture of *E. coli* BL21 (pETyhdA) in LB medium containing ampicillin at 37 °C overnight. The overnight culture was used to inoculate 1 L of fresh LB medium, which was further incubated at 37 °C until the cell density measured as an optical density at 600 nm reached 0.6. At this point, expression of YhdA was induced by the addition of isopropyl-1-thio-D-galactopyranoside (IPTG) to a final concentration of 0.4 mM. Incubation was continued for another 3 h before the cells were harvested by centrifugation. The cell pellet was washed with 0.9% sodium chloride solution and finally stored at −70 °C.

Purification of YhdA and LOT6. The hexahistidine-tagged YhdA was purified by Ni−NTA chromatography. Frozen cells were thawed and resuspended using 2 mL/g wet cells of a 50 mM NaH_2PO_4 buffer containing 300 mM NaCl and

10 mM imidazole (pH 8.0). The cell slurry was subjected to five pulses of sonication for 1 min with intermittent cooling on ice for 1 min. After this treatment, cell debris was removed by centrifugation at 25000*g* for 20 min at 4 °C. The supernatant was applied to a Ni−NTA column (Qiagen), previously equilibrated with lysis buffer. After the sample was loaded, the column was washed with 3 bed volumes of washing buffer (50 mM NaH_2PO_4, 300 mM NaCl, and 20 mM imidazole at pH 8.0). Bound protein was eluted with 50 mM NaH_2PO_4, 300 mM NaCl, and 150 mM imidazole at pH 8.0 and collected in 3 mL fractions. Fractions containing YhdA were pooled and concentrated in Centripreps (Millipore). In this concentration step, the buffer was exchanged to 100 mM Tris-HCl at pH 7.5. The enzyme solution was flash-frozen in liquid nitrogen and stored at −20 °C. The purity of YhdA was estimated by sodium dodecyl sulfate−polyacrylamide gel electrophoresis (SDS−PAGE) to be higher than 95% (*13*).

The expression clone for LOT6 from *S. cerevisiae* was a generous gift of Prof. Herman van Tilbeurgh, University of Paris-Sud, France. Protein expression and purification was done as described in ref *12*.

Enzyme Assays. YhdA activity was measured spectrophotometrically (Analytik Jena, Germany, model Specord 205 equipped with a thermostated cell holder). All reactions were carried out in 100 mM Tris-HCl at pH 7.5 and 37 °C. The reduction of azo dyes was measured in 1 mL cuvettes containing 4 μM YhdA, 1 mM NADPH, 10 μM FMN, and 20 μM dye, if not stated otherwise. Initial rates were determined by monitoring the absorbance decrease at a suitable wavelength (Cibacron Marine, 597 nm). Oxidation of NAD(P)H was monitored at 340 nm at 30 °C. Enzyme activity was calculated by using a molar absorption coefficient of 6220 and 44 700 M^{-1} cm^{-1} for NADPH and Cibracron Marine, respectively.

The temperature dependence of the enzyme activity was measured with Cibacron Marine as a model substrate in 100 mM Tris-HCl at pH 7.5 containing 4 μM YhdA and 20 μM Cibacron Marine using a temperature range of 10−80 °C. The temperature inactivation of YhdA was determined by heating the enzyme for 10 min at a certain temperature (20−90 °C). After incubation, the enzyme was equilibrated for 1 min at 37 °C and the residual activity was determined using Cibacron Marine as the substrate.

Spectrophotometric Methods. YhdA-bound FMN was released by the addition of 0.2% SDS. UV−vis absorbance spectra were recorded before and after denaturation of the enzyme.

Oxygen Measurements. The simultaneous measurement of the UV−vis absorbance and the oxygen content was achieved by fitting a Microx TX3 fiberoptic oxygen microsensor (140 μm glass fiber, PreSens) to the cuvette. Dynamic quenching of luminescence by molecular oxygen was used to sense the concentration of dissolved oxygen using an oxygen microsensor prepared as described by Holst et al. (*14*). Calibration of the sensor was performed by using a two-point calibration in air-saturated 100 mM Tris-HCl at pH 7.5 buffer (=100% dissolved oxygen) and buffer containing 10 g of Na_2SO_3/100 mL (=0% dissolved oxygen).

Photoreduction. YhdA was photoreduced anaerobically using a 50 W halogen lamp as a light source. Anaerobic conditions were established by repeated cycles of evacuation and flushing with oxygen-free nitrogen gas. Solutions contained 40 μM YhdA in 100 mM Tris-HCl buffer at pH 7.5.

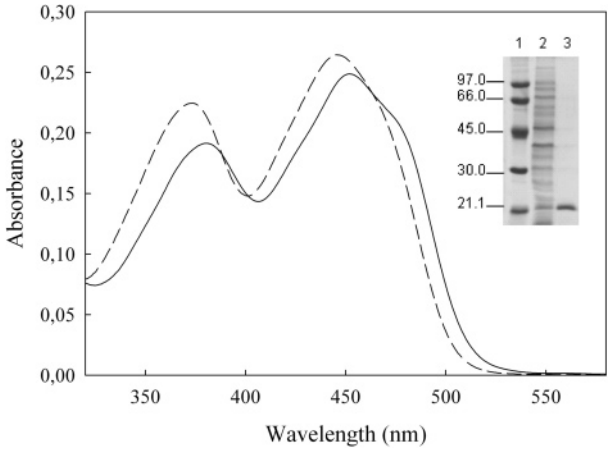

FIGURE 1: UV−vis absorbance spectrum of YhdA before and after denaturation. Solid and dashed lines represent the spectrum of YhdA and free FMN, respectively. Denaturation of purified YhdA was carried out in storage buffer (100 mM Tris-HCl at pH 7.5) containing 0.2% SDS. The inset shows SDS−PAGE of YhdA expression and purification. Lane 1, molecular-mass standard as indicated; lane 2, protein extract after induction of YhdA; and lane 3, purified protein YhdA. Proteins were visualized by Coomassie Blue staining.

Native Molecular-Weight Determination. To assess the oligomerization state of native YhdA, we determined the molecular mass of the purified protein using molecular sieve chromatography on a Superdex 200 10/300 GL column (Pharmacia Biotech AB). The analytical column was mounted on a fast protein liquid chromatography (FPLC) system (ÄKTA Explorer, Pharmacia Biotech AB). The column was equilibrated with 100 mM Tris-HCl buffer containing 150 mM NaCl at pH 7.5. A 1 mL sample containing 200 μg of YhdA was applied to the column, and the elution volume was determined by monitoring the absorbance at 280 and 450 nm. The column was previously calibrated using a high-molecular-mass gel-filtration calibration kit [Amersham Biosciences; α-chymotrypsinogen A, 25 kDa; ovalalbumin, 43 kDa; bovine serum albumin (BSA), 67 kDa; aldolase, 158 kDa; catalase, 232 kDa; and ferritin, 440 kDa].

Thermal Unfolding Experiments. Thermal unfolding of YhdA was monitored in 0.1 cm cuvettes using a Jasco J-500 spectropolarimeter at 225 nm. The cuvette was placed in a thermostated cell holder. The temperature was raised continuously from 5 to 95 °C at a heating rate of 1.0 °C/min. The enzyme concentration was 57 and 37 μM for LOT6 and YhdA, respectively, in 100 mM Tris-HCl at pH 7.5.

RESULTS

Cloning of *yhd*A into the IPTG-inducible expression vector pET21a and transformation of *E. coli* BL21 (DE3) cells lead to the expression of YhdA that amounts to a sizable fraction of the total soluble protein (inset of Figure 1). Because YhdA is expressed as a C-terminally hexahistidine-tagged protein, it could be purified to near homogeneity by a one-step Ni−NTA-affinity chromatography, yielding about 3 mg of YhdA from 20 g of wet biomass. The UV−vis absorbance spectrum of YhdA shows two distinct peaks at 375 and 455 nm, clearly indicating the presence of a flavin cofactor (Figure 1). This

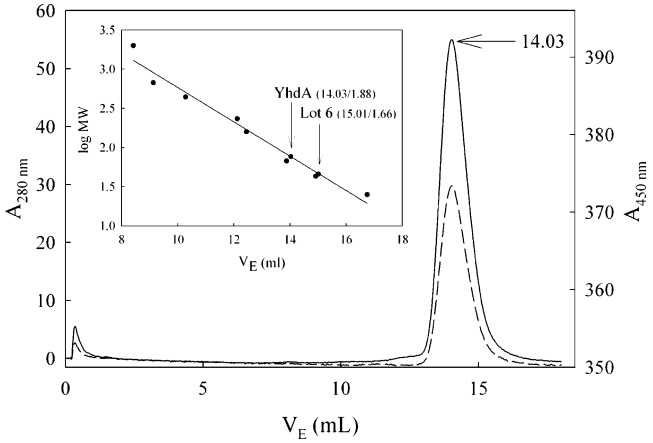

FIGURE 2: Determination of the native molecular weight of YhdA by gel-filtration chromatography. A single protein species is detected upon FPLC chromatography (Superdex 200 10/300 GL) of purified YhdA. The lines represent the absorbance at 280 nm (—) and 450 nm (- - -), respectively. The inset shows the calibration curve and calculation of the molecular weight for native YhdA and LOT6. Molecular-weight marker proteins were α-chymotrypsinogen A (25 kDa), ovalalbumin (43 kDa), BSA (67 kDa), aldolase (158 kDa), catalase (232 kDa), and ferritin (440 kDa).

finding is in agreement with the three-dimensional structure of the enzyme (PDB entry code 1NNI), showing a noncovalently bound FMN molecule. The release of the cofactor by denaturation of the protein produced a hypochromic shift of both absorbance maxima to 350 and 450 nm, respectively, characteristic of free FMN. Using an extinction coefficient of $\epsilon_{450} = 12\,400\ M^{-1}\ cm^{-1}$ for free FMN, the extinction coefficient for FMN bound to YhdA was determined to $\epsilon_{455} = 11\,780\ M^{-1}\ cm^{-1}$.

The native molecular weight of YhdA was determined by size-exclusion chromatography, generating a single peak indicative of a stable oligomeric complex (Figure 2). The elution volume corresponds to a molecular weight of 76 kDa, demonstrating that YhdA forms a homotetramer in solution. This result is in agreement with the determined X-ray crystal structure of YhdA, which predicts a homotetrameric assembly of the protein (Macromolecular Structure Database, http://pqs.ebi.ac.uk). In contrast to YhdA, the homologous yeast protein LOT6 was reported to form a homodimer, which is supported by size-exclusion chromatography (inset of Figure 2).

To further characterize the properties of YhdA, the enzyme was subjected to photoreduction under anoxic conditions (Figure 3). During illumination, the flavin chromophore is gradually reduced to the fully reduced (dihydroquinone) form without any indication of the occurrence of a flavin semiquinone radical. After complete reduction, the oxidized form of FMN could be fully restored by reoxidation with dioxygen (top trace of Figure 3).

Alternatively, YhdA is also reduced by NADH and NADPH, with a clear preference for NADPH as shown in Figure 4. Although the apparent K_m for NADH and NADPH, estimated to 0.65 and 0.55 mM, respectively, are similar, the rate of reduction is 80 times faster with NADPH, indicating that this is the likely physiological reducing agent of YhdA. Reduction of YhdA was further studied by the analysis of initial rates of NADPH oxidation as a function of the FMN concentration. As shown in Figure 5, the rate of NADPH oxidation increases with increasing FMN con-

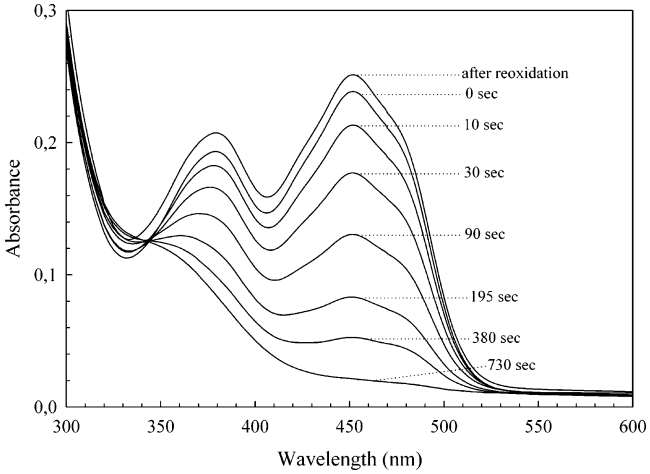

FIGURE 3: Photoreduction of YhdA. YhdA [40 μM enzyme in 100 mM Tris-HCl buffer at pH 7.5 and 1 mM ethylenediaminetetraacetic acid (EDTA)] was made anaerobic by repeated cycles of evacuation and flushing with oxygen-free nitrogen gas. The second spectrum from the top shows the absorbance spectrum of YhdA after establishing anaerobic conditions (time = 0 s). Thereafter, the sample was photoreduced using a 50 W halogen lamp as a light source. Further spectra represent illumination periods of 10, 30, 90, 195, 380, and 730 s, respectively. The top spectrum was recorded after complete photoreduction and reoxidation by dioxygen to the fully oxidized species.

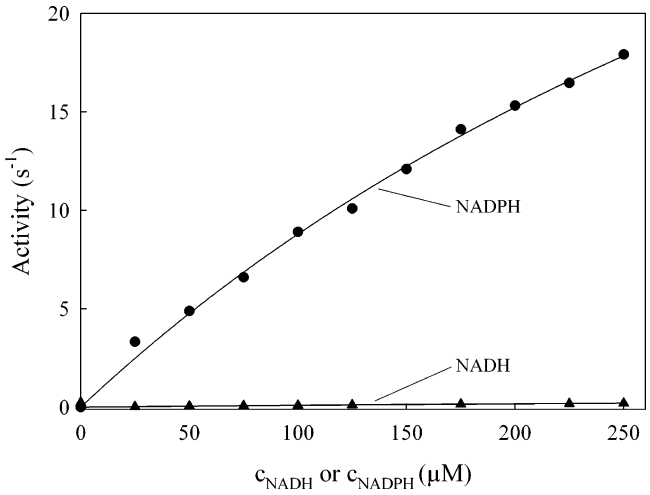

FIGURE 4: Oxidation of NADH and NADPH by YhdA in the presence of FMN. The oxidation of NADH (▲) and NADPH (●) was recorded at 340 nm in the presence of 10 μM FMN. When a nonlinear hyperbolic Michaelis−Menten equation was applied, the obtained data points could be fitted yielding a v_{max} of 0.7 and 57 s^{-1} and K_m of 0.65 and 0.55 mM for NADH and NADPH, respectively.

centrations producing a family of lines, which intersect on the $-1/x$ axis, yielding a K_m value of 0.58 mM for NADPH (Figure 5A). A replot of the data in Figure 5 with FMN as the variable substrate (concentration on $1/x$ axis) and NADPH as the fixed variable substrate also yields a family of lines intersecting above the −1/FMN axis, giving a K_m value of 20 μM for FMN (Figure 5B). To derive k_{cat} values, the *y*-axis intercepts in parts A and B of Figure 5 were plotted against the reciprocal concentration of the fixed variable substrate. As can be expected, this procedure yields similar k_{cat} values for FMN reduction and NADPH oxidation of 60 and 70 s^{-1}, respectively. It should be noted in this context that the concentration range of NADPH is below the K_m value determined from the experiment shown in Figure 4, and

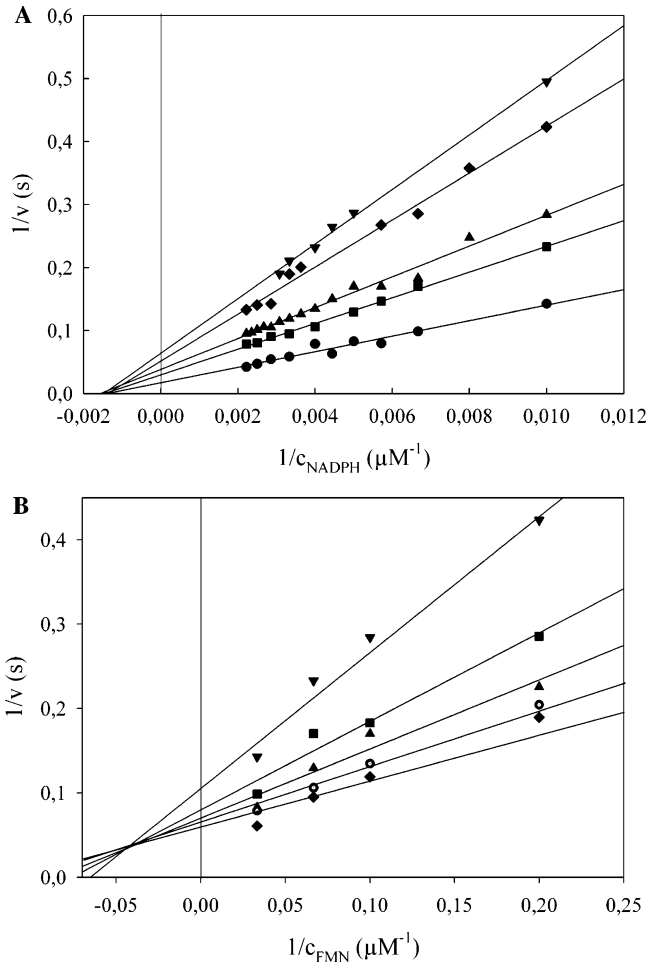

FIGURE 5: Rate of NADPH oxidation as a function of the FMN concentration. (A) Double-reciprocal plot of initial velocities (v) versus concentrations of NADPH (100−500 μM) measured at 340 nm. The NADPH oxidation activity was assayed at 37 °C at varying concentrations of FMN. FMN concentrations used were 2 μM (▼), 5 μM (◆), 10 μM (▲), 15 μM (■), and 30 μM (●). (B) Replot of the data from A. NADPH concentrations were 100 μM (▼), 150 μM (■), 200 μM (▲), 250 μM (○), and 300 μM (◆).

hence, the derived kinetic parameters should be regarded as estimates.

The result of our kinetic analysis is characteristic for the occurrence of a ternary complex in a bi-bi ternary mechanism; i.e., both FMN and NADPH must bind to the active site of YhdA before catalysis can occur. Basically, the formation and dissociation of the ternary complex can follow an ordered or random mechanism or a combination of both. Initial velocity measurements cannot discriminate between these two possibilities. This would be possible by the analysis of the inhibition kinetics of specific inhibitors directed against the FMN- or NADPH-binding site (*15*). However, such inhibitors are currently not known for YhdA.

The observation of a ternary complex of YhdA, FMN, and NADPH could also imply that the copurified FMN cofactor dissociates from the active site after reduction by NADPH; in other words, the YhdA as isolated can be regarded as the YhdA/FMN binary complex. Alternatively, YhdA possesses yet another FMN-binding pocket, where a second FMN molecule must bind to form the ternary complex with NADPH. To distinguish between these two scenarios, we have bound the histidine-tagged YhdA to a Ni−NTA column and then reduced the protein by treatment of a buffer

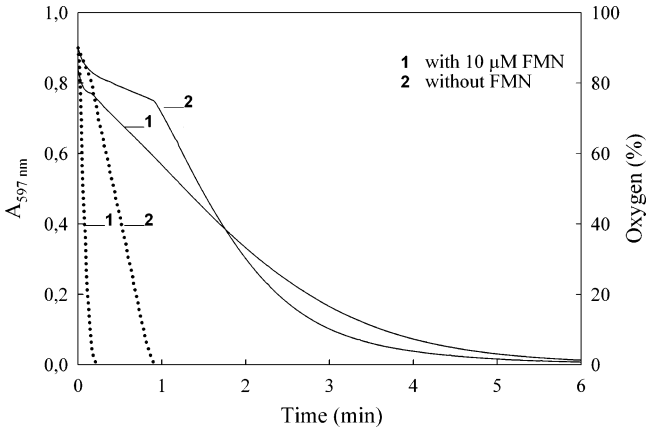

FIGURE 6: Influence of dissolved oxygen on the rate of dye reduction. Reduction of Cibacron Marine was determined spectrophotometrically at 597 nm. Solid lines represent the degradation of the azo dye in the presence and absence of external FMN, respectively (1, with 10 μM FMN; 2, without FMN). Reduction of dioxygen is represented by the dotted lines in the presence and absence of external FMN as indicated before.

containing 1 mM NADPH until the enzyme was fully reduced, which is readily observable by the complete loss of the yellow color of YhdA. After YhdA was extensively washed with this reducing buffer, it was eluted from the affinity resin and a UV−vis absorbance spectrum of the protein fraction was recorded. The OD_{280}/OD_{450} is a convenient measure to determine the ratio of protein/FMN, and this ratio was unaltered after this treatment, indicating that no loss of FMN has occurred during this procedure. This finding confirms that FMN does not dissociate from the binding pocket upon reduction by NADPH. Additional support is provided by the X-ray crystal structure of YhdA, which shows a deeply buried ribityl phosphate side chain anchoring the cofactor tightly to the protein (PDB entry code 1NNI).

The homologous enzyme from *Bacillus* sp. OY1-2 was reported to reduce azo dyes (*4*), and hence, we were interested in testing the ability of YhdA to catalyze the reduction of our model azo dye Cibacron Marine. The reduction process can be monitored by following the loss of absorbance of the dye that results from the reductive cleavage of the −N═N− bond to the corresponding free amino products (see the scheme in the Introduction). As can be clearly seen in Figure 6, this process possesses at least two discernible phases, a slow reduction process at the beginning followed by a more rapid one (— in Figure 6). The initial lag phase was found to correlate with the removal of dissolved oxygen in the sample (⋯ in Figure 6). In other words, dioxygen serves as an alternative electron acceptor, and as soon as it is consumed, reduction of the dye occurs at a faster rate. The consumption of dioxygen can be accelerated by the addition of external FMN (dotted trace 1 in Figure 6), in which case the lag phase is shortened and dye reduction occurs earlier (solid trace 1 in Figure 6). However, dye reduction appears to be slower after the lag phase in the presence of FMN (compare solid traces in Figure 6), indicating an inhibitory effect of FMN upon dye reduction.

To gain further information on the interference of FMN and dye reduction, we performed initial rate measurements of NADPH oxidation as a function of NADPH and Cibacron

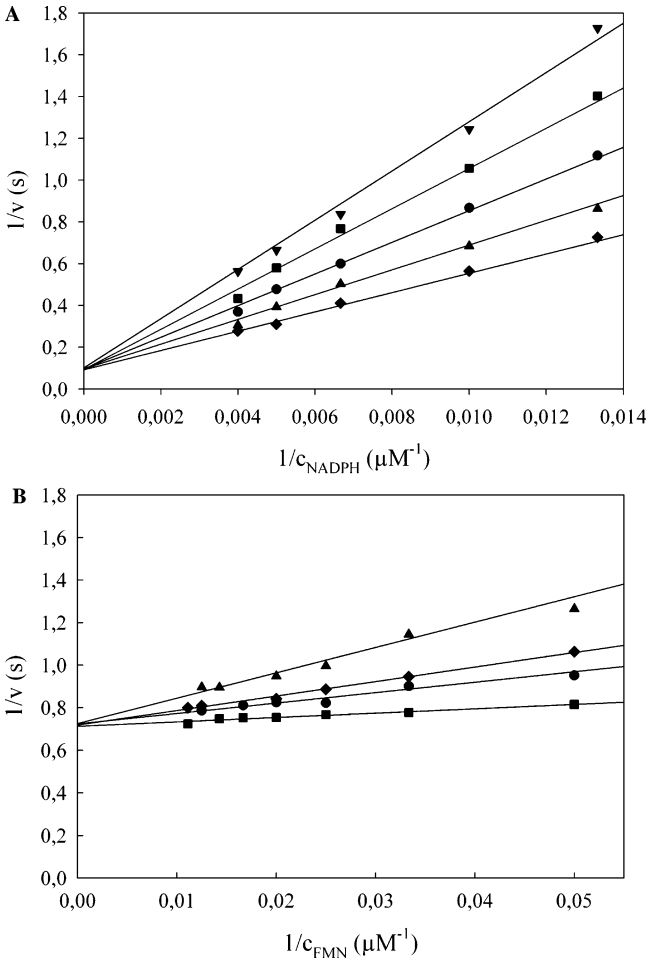

FIGURE 7: (A) Double-reciprocal plots of the initial velocity (v) versus the concentration of NADPH (80−250 μM) at a fixed concentration of 10 μM FMN and varying concentration of Cibacron Marine. Concentrations of the dye were 5 μM (◆), 10 μM (▲), 20 μM (●), 30 μM (■), and 40 μM (▼). (B) Double-reciprocal plots of the initial velocity (v) versus the concentration of FMN (20−80 μM) at a fixed concentration of 1 mM NADPH and varying concentrations of Cibacron Marine. Concentrations of the dye were 10 μM (■), 15 μM (●), 25 μM (◆), and 30 μM (▲).

Marine at a fixed concentration of FMN and as a function of FMN and Cibacron Marine at a fixed concentration of NADPH, respectively. The double-reciprocal plots of these experiments are shown in parts A and B of Figure 7, respectively, and indicate that Cibacron Marine is a competitive inhibitor of NADPH and FMN. This type of inhibition pattern is consistent with a rapid-equilibrium random bi-bi mechanism. From a replot of the data in Figure 7, inhibition constants of 15 and ≈3 μM are obtained for the inhibition of NADPH and FMN, respectively. The k_{cat} value found for the reductive degradation of Cibacron Marine is 0.7 s^{-1}, i.e., about 100 times slower than the turnover with FMN (see above). Owing to its slow turnover, the dye is a slow substrate compared to FMN and therefore inhibits the reduction of FMN. In terms of the AZR activity, YhdA shows an approximately 10 times higher turnover with Cibacron Marine as the enzyme, previously characterized from *Bacillus* sp. OY1-2 (*4*). On the other hand, it should be noted that the AZRs isolated from *E. faecalis* and *E. coli* exhibit 20 and 80 times higher turnover rates, respectively (using the azo dye Methyl Red), than YhdA (*5*, *6*).

Table 1: AZR Activity in the Crude Extract Obtained from the *B. subtilis yhd*A Knock-Out Strain *yhd*Ad[a]

azo dye	AZR activity	azo dye	AZR activity
Cibacron Marine	31	Ponceau 2R	102
Orange IV	95	Tartrazine	66

[a] The activity is expressed as the percentage relative to the activity found in crude extracts of *B. subtilis* wild type (strain 168) and is normalized for the protein concentration.

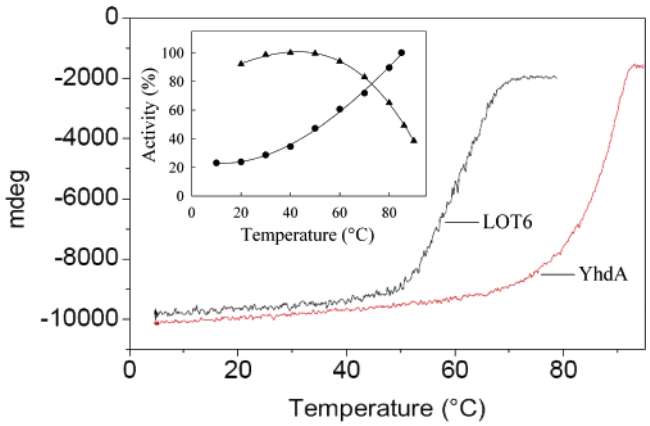

FIGURE 8: Thermal denaturation of YhdA. Thermal unfolding of YhdA was measured by monitoring the CD signal as a function of the temperature (main panel). Thermal stability of the YhdA activity was assessed by incubating the enzyme for 10 min at the temperature indicated (▲ in the inset). The residual activity was determined at 37 °C with Cibacron Marine as a substrate as described before. (●) Activity of the enzyme as a function of the assay temperature.

Following up on the ability of YhdA to reduce azo dyes, we have tested crude extracts obtained from the *yhd*A knock-out strain (termed *yhd*Ad) for its AZR activity. These crude extracts exhibit comparable AZR activity toward several dyes such as Cibacron Marine, Tartrazine, Orange IV, and Ponceau 2R (Table 1). This clearly indicates that other AZRs must exist in *B. subtilis* protein extract and that YhdA does not constitute the major AZR activity.

A higher oligomerization state of a protein has a potential effect on temperature stability (*16*). This prompted us to investigate the temperature stability of the tetrameric YhdA and compare it to that of the homologous dimeric LOT6. Therefore, we have evaluated the thermostability of YhdA in three different experiments (Figure 8). First, we have determined the melting temperature (T_m) of YhdA (and LOT6) by following the denaturation of the protein in a circular dichroism (CD) spectropolarimeter as a function of the temperature (main panel in Figure 8). Second, we measured the initial rate of reductive degradation of our model dye Cibacron Marine as a function of the temperature, and third, residual activity after incubation at a certain temperature was determined (for details, see the Materials and Methods). T_m of YhdA obtained from the first experiment is 86.5 °C (LOT6, T_m = 60.2 °C), and hence, YhdA has an unusually high thermostability for a protein of a mesophilic bacterium. It is also worth mentioning that both proteins are irreversibly denatured in the temperature-scan experiments. This result is also supported by the temperature profile and the temperature inactivation kinetics determined for YhdA (inset of Figure 8).

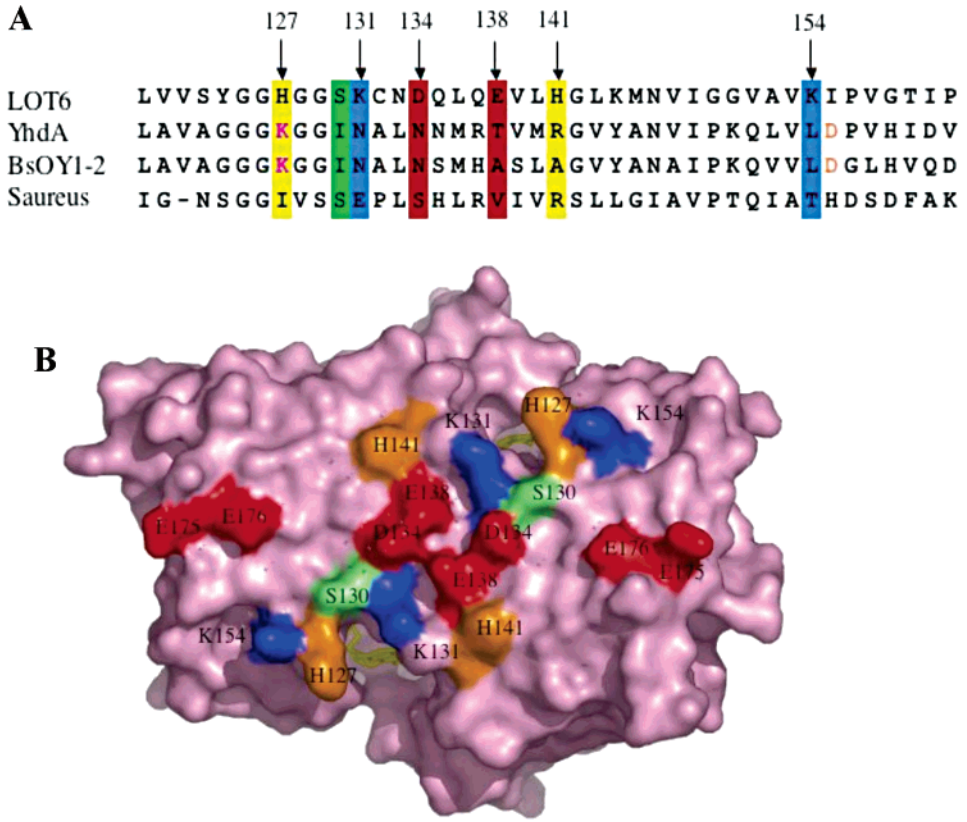

FIGURE 9: Sequence alignment and dimer interface of LOT6. (A) Alignment of the area where most of the charged amino acids on the concave surface formed by the association of two LOT6 monomers occur. The numbering gives the position of the amino acid in LOT6. The three bacterial homologues are from *B. subtilis* (YhdA), *B. subtilis* OY1-2 (BsOY1-2), and *S. aureus* (Saureus). Negatively charged amino acids are highlighted in red; positively charged amino acids are highlighted in blue; histidines are highlighted in yellow; and serine is highlighted in green. Replacements in YhdA that give rise to a salt bridge in the tetramer are shown in magenta and orange letters, respectively. (B) Representation of the extended concave surface generated by dimerization of LOT6, showing the high concentration of charged amino acid residues in the central part. Negatively charged residues are shown in red; positively charged residues are shown in blue; histidines are shown in orange; and serine is shown in green. All other amino acids are shown in light magenta. PyMol was used to generate the graphic.

DISCUSSION

Our measurements have shown that YhdA preferentially uses NADPH as the electron donor to reduce the active-site FMN. Moreover, external FMN is an efficient electron acceptor (see Figures 4 and 5), and hence, YhdA can be classified as a NADPH:FMN oxidoreductase. Typically, these enzymes operate via a bi-bi ping-pong mechanism, where the reductant binds first to the active site to deliver the electrons to the active-site cofactor and then dissociates before the electron-accepting substrate binds to the active site to sequester the electrons (*17*, *18*). This type of mechanism is characterized by a family of parallel lines, which are obtained by plotting initial rates at various concentrations of both substrates in a double-reciprocal fashion. Our analysis of initial rate measurements has generated a family of lines, which intersect in the second quadrant, clearly indicating the formation of a ternary complex; i.e., both substrates must bind simultaneously to the active site of YhdA to achieve catalysis. This finding raises the question where NADPH and FMN could bind to the active site of YhdA. The structure of YhdA and LOT6 possesses a putative nucleotide-binding site at the edge of the pyrimidine ring moiety, which could be used by NADPH to dock to the bound FMN to deliver two electrons to the isoalloxazine ring. Such a binding could be shown in NAD(P)H:quinone reductase, with an FAD-dependent enzyme that was shown to bind $NADP^+$ such that the nicotinamide ring stacks upon the *si* face of the isoalloxazine ring system (*19*). As shown for this enzyme, quinone substrates bind to the same site to accept the electrons from the reduced FAD cofactor, giving rise to ping-pong kinetics. Clearly, in the case of YhdA, the accepting FMN substrate does not bind to the same site as NADPH; however, the exact location of the binding site remains elusive in the absence of structural data. Therefore, future structural studies will focus on the determination of this second binding site for the "external" FMN.

Mechanistic and functional investigations have focused on the ability of these enzymes to reduce azo dyes (*4*, *12*). To develop a better understanding of the dye reduction process, we have used a microsensor for dissolved oxygen in our assay system, demonstrating that reduction of YhdA by NADPH also leads to the reduction of dioxygen (Figure 6). This process is accelerated by addition of external FMN and precedes the reduction of the azo dye. After complete removal of dioxygen from the assay mixture, azo dye reduction occurs at a faster rate. The efficiency of azo dye degradation via reduction of the azo bond is therefore higher in an anoxic environment. On the other hand, YhdA does not appear to be the best choice for an enzymatic degradation system because the model azo compound Cibacron Marine is a competitive inhibitor of NADPH, which in turn is

required for azo dye degradation. In terms of an application in bioremediation, AZRs operating via a ping-pong mechanism could provide more suitable enzymatic systems. AZR activity was also found in crude extracts from a *B. subtilis* YhdA knock out and indicate that other AZRs must be present, which should be identified and tested for their capability for azo dye degradation (see Table 1).

Molecular sieve chromatography has demonstrated that the recombinant enzyme forms a tetramer in solution with an apparent molecular mass of 76 kDa. This result is in agreement with a previous report that a homologous AZR from *S. aureus* also forms a tetramer; hence, it appears that AZRs from Gram-positive bacteria share a tetrameric organization in solution. On the other hand, the yeast homologue LOT6 is shown to form a dimer in solution (Figure 2). The different oligomerization of YhdA and LOT6 was also predicted by the crystallographic analysis of the proteins (*12*; PDB entry codes 1NNI and 1T0I, respectively). This finding is particularly intriguing because YhdA possesses a 26.3 °C higher melting temperature than LOT6 (Figure 8). Increased thermostability of proteins can be achieved by various means such as more efficient packing, an increase in subunit contacts, hydrogen bonding, and ion-pair formation, and formation of higher oligomers. The latter contribution has been described as playing an important role in thermoadaptation (*16*, *20*). Formation of higher oligomers is strongly favored by replacement of charged residues by uncharged residues in the dimerization interface, leading to stronger hydrophobic packing between subunits. For example, the replacement of a single lysine residue to either one of the hydrophobic amino acids leucine, isoleucine, and methionine in the Lac repressor increases thermostability by 40 °C (*21*). The dimeric structure of LOT6 features a large, slightly concave surface characterized by four α helices, which span its entire width (*12*). In the case of LOT6, this surface features several charged residues in its central part, as highlighted in Figure 9B, which would certainly interfere or weaken the interaction between two dimers. In contrast to LOT6, all of these charged residues are replaced by hydrophobic or uncharged residues in YhdA (Figure 9A). This allows the formation of a tetramer by packing the two extended dimer surfaces against each other by a 90° rotation of one dimer with respect to the other (Figure 10). This assembly is further stabilized by the formation of four salt bridges between K109 and D137 (Figure 10). Interestingly, both of these contacts arise from two replacements in YhdA in comparison to the LOT6 sequence (Figure 9A). Therefore, it appears that the formation of a homotetramer is driven by at least two forces, increased hydrophobic packing and formation of ion-pair contacts between two dimers. On the basis of this structural evidence, we propose that tetramerization of YhdA leads to the observed higher apparent thermostability in comparison to the dimeric yeast protein. This hypothesis will be further tested by site-directed mutagenesis of residues proposed to participate in the stabilization of the tetramer.

Both YhdA and LOT6 adopt a typical flavodoxin-like fold consisting of a central five-stranded parallel β sheet sandwiched by α helices on either side (PDB entry codes 1NNI and 1T0I, respectively). Flavodoxins are small monomeric electron transferases, mostly of bacterial origin, which have a FMN cofactor bound in a similar position as YhdA and

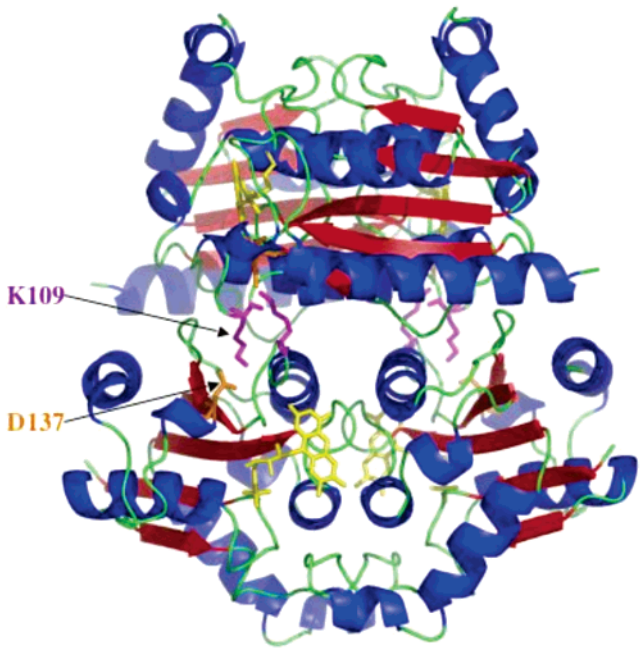

FIGURE 10: Ribbon representation of YhdA generated from a PDB file obtained from the Macromolecular Structure Database (http://pqs.ebi.ac.uk). α helices are shown in blue; β sheets are shown in red; and loops are shown in green. The FMN cofactor is shown in yellow. The homotetramer is stabilized by hydrophobic packing and four salt bridges between K109 (magenta) and D137 (orange). The latter two residues are highlighted in Figure 9A in magenta (at position 127) and orange (at position 155).

LOT6. However, the flavin environment in flavodoxins and YhdA/LOT6 shows pronounced differences with regard to the binding mode of the ribityl phosphate side chain as well as the redox-active isoalloxazine ring. In flavodoxins, a conserved fingerprint sequence T(or S)XTGXT interacts with the ribityl phosphate, while YhdA and LOT6 feature a distinct N-terminal sequence that is involved in the binding of the FMN side chain (*12*). Even more importantly, the isoalloxazine ring experiences a distinct environment in flavodoxins compared to YhdA and LOT6. In the former group of proteins, the *re* and *si* faces of the isoalloxazine ring are shielded by a tryptophan and tyrosine side chain, respectively, and only the edge of the dimethylbenzene ring is accessible (Figure 11). On the other hand, the *si* face of the isoalloxazine ring is readily accessible in YhdA and LOT6 and, additionally, features a nucleotide-binding motif (GGHGG) in the vicinity of the pyrimidine ring. Apparently, this binding site may be utilized by NADPH to reduce the isoalloxazine ring system directly, whereas flavodoxins exchange electrons via direct transfer from and to protein reaction partners via the dimethylbenzene ring moiety (*22*). The interactions with the protein and the burying of the isoalloxazine ring are the structural basis for the most salient property of flavodoxins to shift the midpoint potential of the physiologically relevant semiquinone to the hydroquinone couple from −300 to −520 mV, which results in a thermodynamic stabilization of the (neutral) flavin semiquinone (reviewed in ref *23*). The formation of such a flavin semiquinone is easily detectable by observation of the characteristic spectral changes during photoreduction of flavodoxins (*24*). In the case of YhdA, anaerobic photoreduction of the FMN results in the direct conversion of the oxidized form into the fully reduced hydroquinone form with

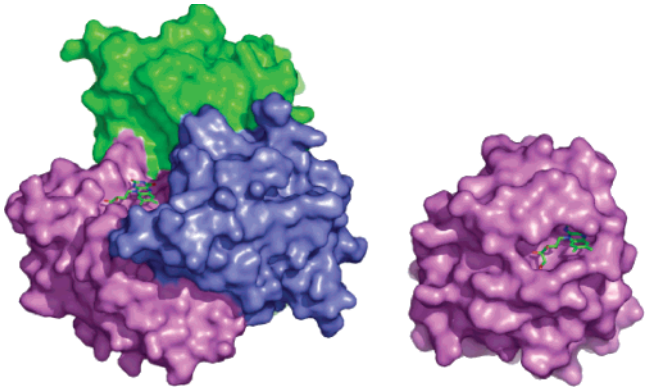

FIGURE 11: Comparison of the FMN-binding pocket of tetrameric YhdA from *B. subtilis* (left) and flavodoxin from *Anacystis nidulans* (right; PDB entry code 1CNZ). The surface of the two monomers contributing to FMN binding of each monomer is shown in violet and blue, respectively. The other two monomers of the tetramer are shown in green. The surface of the monomeric flavodoxin is shown in violet. The flavin is represented by a color-coded stick model (carbon in green, nitrogen in blue, and oxygen in red). The figure was prepared using PyMol.

no indication that a semiquinone occurs during the reduction process (see Figure 3). This clearly demonstrates that flavodoxins and YhdA, despite their common overall protein topology, possess very different redox properties. To shed more light on the redox properties of YhdA and LOT6, we are currently in the process of determining their redox potentials.

The viability of the *yhd*A knock out under standard growing conditions suggests that YhdA is not essential for *B. subtilis*, and hence, a functional role for YhdA cannot be assigned at present. Interestingly, the homologous yeast protein LOT6 has been implicated in the low-temperature response in *S. cerevisiae* (*25*). Likewise, DNA microarray analysis has indicated an approximately 1000-fold increase in the transcript level for YhdA in response to cold shock (http://bacillus.genome.jp). The role of both YhdA and LOT6 will be further investigated by raising antibodies against these proteins to evaluate their role in response to cold shock and possibly other stressors.

ACKNOWLEDGMENT

We thank Prof. Dr. I. Klimant and Dipl.-Chem. Alen Pasic, Institute of Analytical Chemistry, Graz University of Technology, Austria, for their invaluable support using the oxygen microsensor. We are also grateful to Dr. Kobayashi, Nara Institute of Science and Technology, Japan, for providing the *B. subtilis* knock-out strain *yhd*Ad.

REFERENCES

1. Tu, S.-C. (2001) Reduced flavin: Donor and acceptor enzymes and mechanisms of channeling, *Antioxid. Redox Signaling 3*, 881−897.
2. Ernster, L., Estabrook, R. W., Hochstein, P., and Orrenius, S. (1987) DT-diaphorase, a quinone reductase with special functions in cell metabolism and detoxication, *Chem. Scr. 27A*, 1−207.
3. Maier, J., Kandelbauer, A., Erlacher, A., Cavaco-Paulo, A., and Gübitz, G. M. (2004) A new alkali-thermostable azoreductase from *Bacillus* sp. strain SF, *Appl. Environ. Microbiol. 70*, 837−844.
4. Suzuki, Y., Yoda, T., Ruhul, A., and Sugiura, W. (2001) Molecular cloning and characterisation of the gene coding for azoreductase from *Bacillus* sp. OY1-2 isolated from soil, *J. Biol. Chem. 276*, 9059−9065.
5. Chen, H., Wang, R.-F., and Cerniglia, C. E. (2004) Molecular cloning, overexpression, purification, and characterization of an aerobic FMN-dependent azoreductase from *Enterococcus faecalis*, *Protein Expression Purif. 34*, 302−310.
6. Nakanishi, M., Yatome, C., Ishida, N., and Kitade, Y. (2001) Putative ACP phosphodiesterase gene (acpD) encodes an azoreductase, *J. Biol. Chem. 276*, 46394−46399.
7. Blümel, S., and Stolz, A. (2003) Cloning and characterization of the gene coding for the aerobic azoreductase from *Pigmentiphaga kullae* K24, *Appl. Microbiol. Biotechnol. 62*, 186−190.
8. Bin, Y., Jiti, Z., Jing, W., Cuihong, D., Hongman, H., Zhiyong, S., and Yongming, B. (2004) Expression and characteristics of the gene encoding azoreductase from *Rhodobacter sphaeroides* AS1.1737, *FEMS Microbiol. Lett. 236*, 129−136.
9. Chen, H., Hopper, S. L., and Cerniglia, C. E. (2005) Biochemical and molecular characterization of an azoreductase from *Staphylococcus aureus*, a tetrameric NADPH-dependent flavoprotein, *Microbiology 151*, 1433−1441.
10. Blümel, S., Knackmuss, H.-J., and Stolz, A. (2002) Molecular cloning and characterization of the gene coding for the aerobic azoreductase from *Xenophilus azovorans* KF46F, *Appl. Environm. Microbiol. 68*, 3948−3955.
11. Moutaouakkil, A., Zeroual, Y., Dzayri, F. Z., Talbi, M., Lee, K., and Blaghen, M. (2003) Purification and partial characterization of azoreductase from *Enterobacter agglomerans*, *Arch. Biochem. Biophys. 413*, 139−146.
12. Liger, D., Graille, M., Zhou, C.-Z., Leulliot, N., Quevillon-Cheruel, S., Blondeau, K., Janin, J., and van Tilbeurgh, H. (2004) Crystal structure and functional characterization of yeast YLR011wp, an enzyme with NAD(P)H−FMN and ferric iron reductase activities, *J. Biol. Chem. 279*, 34890−34897.
13. Laemmli, U. K. (1970) Cleavage of structural proteins during the assembly of the head of bacteriophage T4, *Nature 227*, 680−685.
14. Holst, G., Glud, R. N., Kuhl, M., and Klimant, I. (1997) A microoptode array for fine-scale measurement of oxygen distribution, *Sens. Actuators, B 38*, 122−129.
15. Segel, I. H. (1993) *Enzyme Kinetics. Behavior and Analysis of Rapid Equilibrium and Steady-State Enzyme Systems*, Wiley Classics Library ed., Wiley, New York.
16. Dams, T., Auerbach, G., Bader, G., Jacob, U., Ploom, T., Huber, R., and Jaenicke, R. (2000) The crystal structure of dihydrofolate reductase from *Thermotoga maritima*: Molecular features of thermostability, *J. Mol. Biol. 297*, 659−672.
17. Morokutti, A., Lyskowski, A., Sollner, S., Pointner, E., Fitzpatrick, T. B., Kratky, C., Gruber, K., and Macheroux, P. (2005) Structure and function of YcnD from *Bacillus subtilis*, a flavin-containing oxidoreductase, *Biochemistry 44*, 13724−13733.
18. Zenno, S., Kobori, T., Tanokura, M., and Saigo, K. (1998) Purification and characterization of NfrA1, a *Bacillus subtilis* Nitro/flavin reductase capable of interacting with the bacterial luciferase, *Biosci. Biotechnol. Biochem. 62*, 1978−1987.
19. Li, R., Bianchet, M. A., Talalay, P., and Amzel, L. M. (1995) The three-dimensional structure of NAD(P)H:quinone reductase, a flavoprotein involved in cancer chemoprotection and chemotherapy: Mechanism of the two-electron reduction, *Proc. Natl. Acad. Sci. U.S.A. 92*, 8846−8850.
20. Walden, H., Bell, G. S., Russell, R. J. M., Siebers, B., Hensel, R., and Taylor, G. L. (2001) Tiny TIM: A small, tetrameric, hyperthermostable triosephosphate isomerase, *J. Mol. Biol. 306*, 745−757.
21. Gerk, L. P., Leven, O., and Müller-Hill, B. (2000) Strengthening the dimerisation interface of Lac repressor increases its thermostability by 40 °C, *J. Mol. Biol. 299*, 805−812.
22. Simondsen, R. P., and Tollin, G. (1980) Structure−function relations in flavodoxins, *Mol. Cell. Biochem. 33*, 13−24.
23. Mayhew, S. G., and Tollin, G. (1992) in *Chemistry and Biochemistry of Flavoenzymes* (Müller, F., Ed.) pp 389−426, CRC Press, Boca Raton, FL.
24. Massey, V., and Palmer, G. H. (1966) On the existence of spectrally distinct classes of flavoprotein semiquinones. A new method for the quantitative production of flavoprotein semiquinones, *Biochemistry 5*, 3181−3189.
25. Zhang, L., Ohta, A., Horiuchi, H., Takagi, M., and Imai, R. (2001) Multiple mechanisms regulate expression of low-temperature responsive (LOT) genes in *Saccharomyces cerevisiae*, *Biochem. Biophys. Res. Commun. 283*, 531−535.

BI052478R